PCCP

Cite this: *Phys. Chem. Chem. Phys.*, 2012, **14**, 5662–5671

www.rsc.org/pccp

PAPER

Stability of sputter-deposited gold nanoparticles in imidazolium ionic liquids

Evert Vanecht,[a] Koen Binnemans,*[a] Sergiy Patskovsky,[b] Michel Meunier,[b] Jin Won Seo,[c] Linda Stappers[c] and Jan Fransaer[c]

Received 22nd November 2011, Accepted 20th February 2012
DOI: 10.1039/c2cp23677j

The stability of gold nanoparticles synthesised by sputter deposition has been studied *in situ* in 1-butyl-3-methylimidazolium ionic liquids with bis(trifluoromethylsulfonyl)imide, tetrafluoroborate, hexafluorophosphate and dicyanamide anions with UV-VIS absorption spectroscopy and transmission electron microscopy. Besides the growth of the gold nanoparticles, two other processes were observed after sputtering, namely aggregation and sedimentation of these nanoparticles. To model the absorption spectra of the sputtered gold nanoparticles, generalized multiparticle Mie calculations were performed. These theoretical calculations confirm the increase in absorbance at longer wavelength for larger aggregates and are in agreement with the experimental observations. It was found that the kinetics of aggregation and sedimentation scale with the viscosity of the ionic liquid. Small amounts of water were found to have a large detrimental influence on the stability of the colloidal suspensions of the gold nanoparticles in ionic liquids. From the large discrepancy between the theoretical and the experimentally observed stability of the NPs, it was concluded that structural forces stabilize the gold nanoparticles. This was also borne out by AFM measurements.

Introduction

The use of ionic liquids (ILs) for the synthesis of metal nanoparticles (NPs) offers several advantages over water or organic solvents.[1–3] Because of their unique properties such as a highly ionic environment,[4] low vapour pressure,[5] wide liquidus range, wide electrochemical window and pre-organized structure,[6] ionic liquids can be used for applications where conventional solvents fail. An important aspect in the research of NPs in ILs is the stability of the NPs/IL colloidal systems. There is currently a dispute in the literature regarding the stability of metal nanoparticles in ILs. Several research groups show that gold nanoparticles are unstable in ionic liquids without the addition of stabilizers or functionalized ionic liquids,[7–9] while other researchers describe stable gold nanoparticle suspensions in ionic liquids.[10–12] It is known that impurities in ionic liquids have a large influence on the stability of nanoparticles dispersed in ionic liquids.[13] A theoretical estimation of the colloidal interaction between bare monodisperse silica particles, by using the Derjaguin–Landau–Verwey–Overbeek (DLVO) theory,[14,15] indicated that these particles cannot be stabilized by ionic liquids and that they rapidly form aggregates.[16]

One of the issues in studying the stability of metal nanoparticles in ionic liquids is the presence of impurities in the IL/NPs system. In most cases the metal nanoparticles are synthesized by reduction of an organometallic precursor (*i.e.* $AuCl_4$ reduced by $NaBH_4$), introducing unwanted impurities in the ionic liquid. Novel synthesis methods take advantage of the extremely low vapour pressure of ionic liquids, so that the preparation of nanoparticles can be performed at low pressure or even under high vacuum conditions.[17] Torimoto and co-workers reported a method for the synthesis of gold nanoparticles by *sputter deposition*, where gold atoms, knocked out from a gold target cathode by the argon ions, were deposited on an ionic liquid.[18] We recently described the formation and growth of gold nanoparticles prepared by sputtering on an ionic liquid.[19] Dupont and co-workers investigated the influence of the ionic liquid on the shape of the sputter-deposited nanoparticles.[20] Generally, sputter deposition is a very clean synthesis method, because it does not introduce other chemical species. The nanoparticles prepared by this method were found to be very stable, even in the absence of stabilizing agents.[18] Recently, two publications about the stability of metal nanoparticles prepared by a physical vapour deposition technique in which the metal was

[a] *KU Leuven – University of Leuven, Department of Chemistry, Celestijnenlaan 200F, P.O. Box 2404, B-3001 Heverlee, Belgium. E-mail: Koen.Binnemans@chem.kuleuven.be; Fax: +3216327992; Tel: +3216727446*
[b] *École Polytechnique de Montréal, Department of Engineering Physics, Case Postale 6079, Montréal, Québec, Canada*
[c] *KU Leuven – University of Leuven, Department of Metallurgy and Materials Engineering (MTM), Kasteelpark Arenberg 44, P.O. Box 2450, B-3001 Heverlee, Belgium*

evaporated at high temperature and condensed on the ionic liquid surface were published.[21,22]

During our investigation of the influence of the ionic liquid composition on the size and size distribution of gold nanoparticles prepared by sputter deposition, we observed that the stability of the prepared nanoparticle suspensions was a critical point. This paper reports on the stability of these nanoparticles in the bulk phase of imidazolium ionic liquids with different anions. This work tries to improve the understanding of the stability of NPs in ionic liquids.

Experimental details

The ionic liquids 1-butyl-3-methylimidazolium dicyanamide $[C_1C_4Im][N(CN)_2]$ (>98%), 1-butyl-3-methylimidazolium bis(trifluoromethylsulfonyl)imide $[C_1C_4Im][Tf_2N]$ (99%), 1-butyl-3-methylimidazolium tetrafluoroborate $[C_1C_4Im][BF_4]$ (99%) and 1-butyl-3-methylimidazolium hexafluorophosphate $[C_1C_4Im][PF_6]$ (99%) were purchased from IoLiTec. $[C_1C_4Im][N(CN)_2]$ and $[C_1C_4Im][Tf_2N]$ were dried at a *Schlenk* line (2×10^{-2} mbar) at 110 °C for 3 hours with stirring. $[C_1C_4Im][BF_4]$ and $[C_1C_4Im][PF_6]$ were dried at more moderate conditions, first at 40 °C for 2 hours to remove most of the water and then another 3 hours at 90 °C, to prevent hydrolysis of the anions, leading to the formation of hydrogen fluoride. Coulometric Karl Fischer titrations (Mettler-Toledo DL 39 Karl Fischer Coulometer) showed that the water content of the dried ionic liquids was less than 30 ppm.

The sputter experiments were performed using a Bal-Tec SCD 005 sputter coater with a gold foil target. An argon pressure of 0.1 mbar, an electric current of 50 mA, a sputter time of 1 minute and a target–substrate distance of 4 cm were applied, unless otherwise specified. An aliquot of the ionic liquid (3.5 mL) was poured in a PTFE container (40 mm diameter and 6 mm deep) that was placed horizontally on the sputter table. To avoid contamination of the ionic liquids with water, the sputter experiments were performed with the sputter coater placed inside a glove box (<2 ppm of water).

UV-VIS absorption spectra were recorded between 200 and 800 nm at room temperature on a Varian Cary 5000 spectrophotometer. For the spectroscopic measurements, the ionic liquid containing the nanoparticles was poured into a quartz cuvette with an optical path length of 10 mm. The NPs were studied using a Philips CM 200 FEG transmission electron microscope (TEM) operating at an acceleration voltage of 200 kV. The sample was prepared by dipping a copper grid (300 mesh) covered with a lacey carbon film (Agar Scientific) into the ionic liquid containing gold NPs and by draining the excess of ionic liquid with filter paper. The viscosity of the ionic liquids was determined with a Brookfield DV-II + Pro cone/plate set-up viscometer at a temperature of 21 °C. The gold concentration in the sputtered ionic liquids was determined by total-reflection X-ray fluorescence (TXRF) with a S2 Picofox (Bruker AXS, Berlin, Germany). A mixture of acetone and water (50 : 50 vol%) was added to 1 g of the sputtered ionic liquid, to get a final volume of 20 mL. 10 μL of an aqueous 1000 ppm Cu solution was added as an internal standard to 990 μL of the IL/Au/acetone/water suspension. After mixing, 10 μL of this solution was transferred onto a TXRF quartz glass sample carrier and dried in an oven at 100 °C for 10 min. AFM force measurements between a freshly cleaved mica substrate and a Si_3N_4 tip (NP-20 Digital Instruments, k = 0.06 N m^{-1}, radius = 20–60 nm in ionic liquids) were performed using a contact mode Nanoscope III (Digital Instruments). All measurements were done at room temperature.

In the generalized multiparticle Mie (GMM) solution method, developed by Xu *et al.*, the near-field Mie scattering fields of all neighboring particles are superimposed on the external plane-wave interacting with the central particle.[23,24] This makes the GMM method very suitable for the modelling of extinction spectra of clusters of spheres. The extinction of an aggregate of gold nanoparticles in the liquid medium was calculated for two orthogonal polarizations. The refractive index of gold from Johnson and Christy was used.[25]

Results

Coagulation and sedimentation

Gold nanoparticles were synthesized by physical vapour deposition (sputtering) directly on an ionic liquid. The sample was shaken and stirred after sputtering to obtain a homogeneous suspension and was kept in a sealed quartz cuvette. The samples were stored in a glove box (<2 ppm water) to keep the samples dry. Gold nanoparticles were selected as the model system, because of their inertness and because they have been studied in a broad range of media and synthesised by various experimental techniques.[26,27]

The sputtered gold/IL suspensions changed colour as a function of time. In all experiments, the following trend was observed: immediately after sputtering, the suspension had a brown colour or brownish black when a higher amount of gold was sputtered. After a few hours or days (depending on the viscosity of the IL), the colour gradually changed to red, characteristic for gold NPs. Subsequently, the suspension turned purple and, finally, the colour became lighter and a black sediment could be observed at the bottom of the cuvette. The colour change of the sputtered gold/IL suspensions was investigated with UV-VIS absorption spectroscopy. Fig. 1 shows the UV-VIS absorption spectra of gold-sputtered $[C_1C_4Im][N(CN)_2]$ as a function of time after ending the sputtering process. The appearance of a surface plasmon resonance (SPR) band around 530 nm, typical for gold nanoparticles, can be seen and is responsible for the characteristic red colour of a sol of gold NPs.[28]

For transmission electron microscopy (TEM), samples were taken from the bulk ionic liquid containing the gold nanoparticles at the same time as the recording of the absorption spectra. In Fig. 2, the TEM images of $[C_1C_4Im][N(CN)_2]$ after different time intervals are shown. After 2 hours, mainly isolated nanoparticles are observed. After 6 hours, small aggregates can be observed. After 24 hours, larger aggregates with sizes of 200 nm are observed.

The sputtered gold in our samples is present in different forms, ranging from small primary clusters (<2.5 nm) to larger NPs (4–7 nm).[19] Additionally, the larger particles can be present as single NPs or as aggregates with varying sizes (10–800 nm). The amount of coagulation of the larger gold

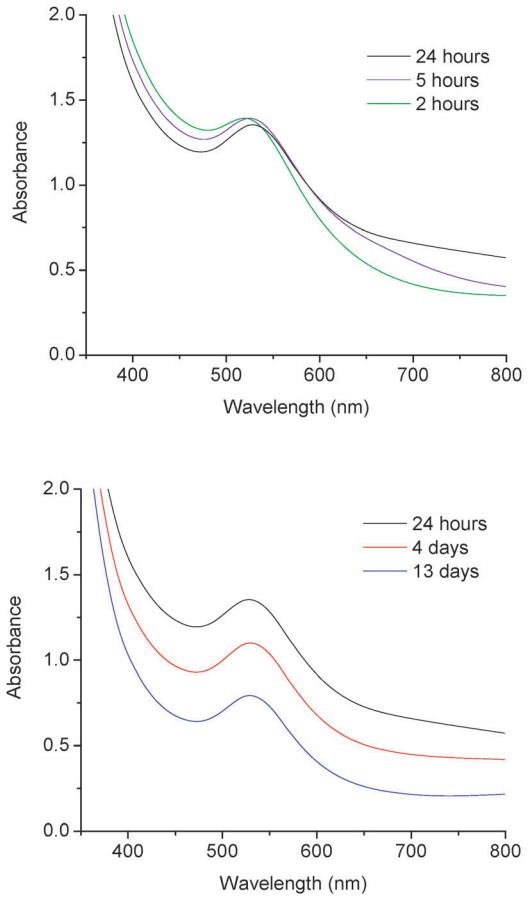

Fig. 1 UV-VIS absorption spectra of gold nanoparticles dispersed in the ionic liquid $[C_1C_4Im][N(CN)_2]$ as a function of time after sputter deposition. The spectra have been recorded at room temperature in a closed quartz cuvette: coagulation (top) and sedimentation (bottom).

NPs (4–7 nm) at different time intervals was estimated. The increase in absorbance around 700 nm in Fig. 1 gives an indication about the rate of coagulation, *i.e.* the kinetic (in)stability of the suspension. Zhong *et al.* performed electrodynamic calculations for gold NPs.[29] These calculations showed that a second SPR peak at longer wavelength arises from interparticles plasmon coupling when gold NPs approach each other within a few nm, usually less than 2 times the particle diameter. The peak wavelength of this second plasmon lies between 550 nm and 750 nm, depending on the interparticle distance, the size of the NPs and the aggregate size. In Fig. 3 the UV-VIS absorption spectra of $[C_1C_4Im][N(CN)_2]$ were fitted using PeakFit®. It can be observed that the large peak around 530 nm increases in absorption in the first 2 hours and stays nearly constant after that. This is due to the growth of small primary NPs to larger NPs during the first hours after sputtering.[19] In contrast, the smaller peaks between 600 to 800 nm are becoming larger and shift to longer wavelengths during 24 hours.

Electrodynamic calculations were performed on aggregates of gold NPs with a diameter of 6 nm in $[C_1C_4Im][N(CN)_2]$ with a refractive index of 1.51 (Fig. 4). For a linear array of gold NPs with 0.5 nm interparticles distance we find that the dipole plasmon resonance of a single particle starts out at 530 nm, then moves to 580 nm for two NPs, to 607 nm for 4 NPs array, then shows saturation at 646 nm for aggregates larger than 40 NPs (Fig. 4, top). For cubic aggregates, it is found that a second peak in the extinction spectrum appears when the aggregates contain more than 10^3 NPs (Fig. 4, bottom). This second peak corresponds to coupled dipole plasmon excitation in the cubic aggregates.

Influence of the ionic liquid anion

The influence of different ionic liquids, $[C_1C_4Im][N(CN)_2]$, $[C_1C_4Im][Tf_2N]$, $[C_1C_4Im][BF_4]$ and $[C_1C_4Im][PF_6]$, on the stability of gold nanoparticle colloids was investigated. Fig. 5 shows the UV-VIS absorption spectra as a function of time after sputtering for the different ionic liquids tested. In Fig. 6, the decrease in absorbance at wavelength 520 nm is plotted as a function of time. For the sake of comparison, the starting time and starting absorbance are both set to zero from the moment that sedimentation started. For $[C_1C_4Im][N(CN)_2]$ and $[C_1C_4Im][Tf_2N]$ the sedimentation started after 1 day. For $[C_1C_4Im][BF_4]$ and $[C_1C_4Im][PF_6]$ the sedimentation started after 5 days, and 9 days, respectively.

Influence of water

All the experiments and results reported so far in this paper were performed with an ionic liquid sample kept dry during the experiments. The ILs were dried on a *Schlenk* line to a water content of less than 30 ppm and were kept in a glove-box

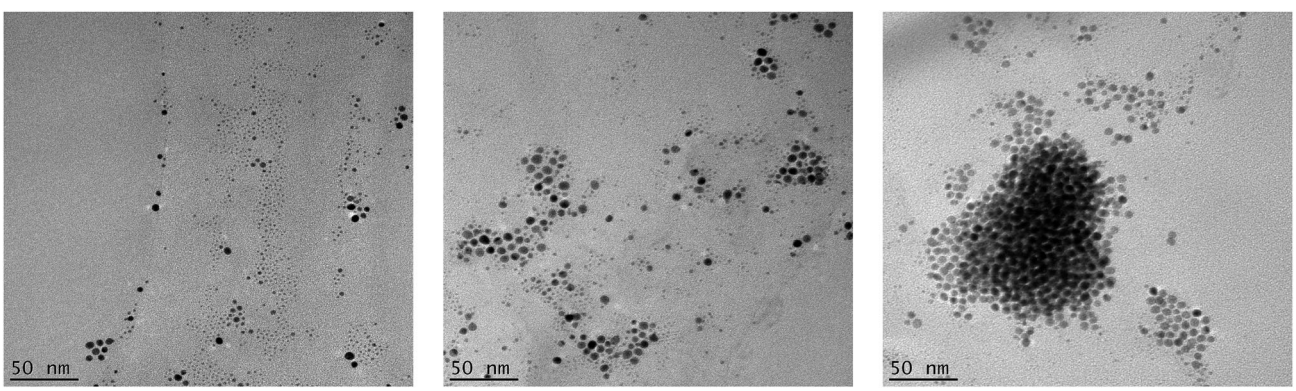

Fig. 2 The representative TEM images of gold nanoparticles in the ionic liquid $[C_1C_4Im][N(CN)_2]$ obtained 2 hours (left), 6 hours (middle) and 24 hours after sputtering (right).

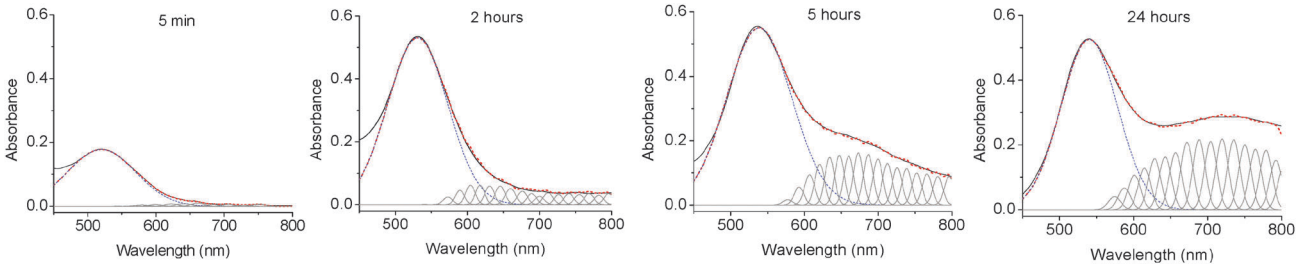

Fig. 3 Experimental UV-VIS absorption spectra of gold nanoparticles dispersed in the ionic liquid $[C_1C_4Im][N(CN)_2]$ as a function of time after sputter deposition. The spectra are fitted using Peakfit®. Experimental absorption spectra (—), total sum of fit (- - -), coupled SPR fit (——), single SPR fit (- - -).

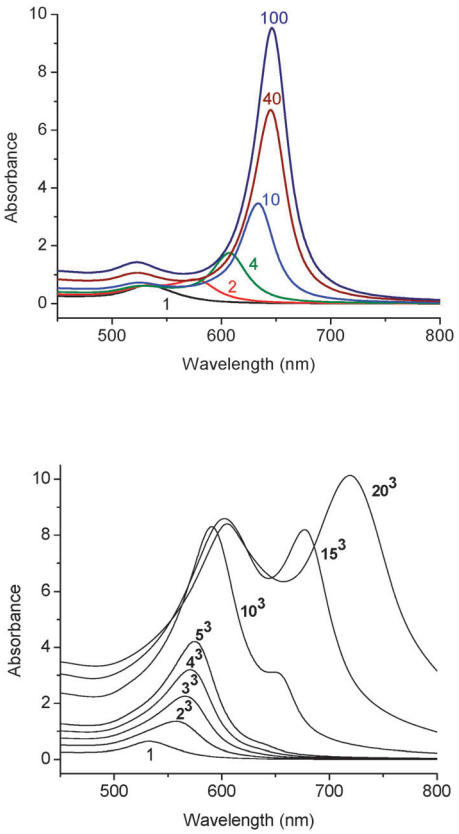

Fig. 4 Calculated extinction curves for linear aggregates for 1–100 NPs (top). Extinction for cubic aggregates with 2^3–20^3 NPs (bottom). All calculations were done for spherical gold nanoparticles with a diameter of 6 nm and an interparticle distance of 0.5 nm.

after sputtering. When these precautions were not taken, atmospheric moisture could enter the sample.

As a result, the colloids coagulated and sedimented much faster. Fig. 7 compares the UV-VIS absorption spectra of gold nanoparticles dispersed in the ionic liquid $[C_1C_4Im][N(CN)_2]$ kept (i) open to air and (ii) in the glove-box as a function of time. The ionic liquid was dried to a water content of 30 ppm prior to sputtering. The IL needs to be carefully dried before the sputter experiment, otherwise it takes too long for the pressure to decrease to a value low enough for formation of a plasma in the vacuum chamber of the sputter coater. After sputtering, the batch was kept in a cuvette open to the air. Analogous to the dry suspension, coagulation and sedimentation were observed, but in the presence of water the aggregation and sedimentation occurred faster and more intense.

The influence of small amounts of water (ppm range) was investigated in more detail. $[C_1C_4Im][Tf_2N]$ was dried at 120 °C for 24 hours at 10^{-2} mbar. The final water content determined by coulometric Karl Fischer titration was 2 ppm.

An ionic liquid batch containing 10 ppm of water was prepared by drying the ionic liquid on a *Schlenk* line for 6 hours at 80 °C at 10^{-2} mbar. Gold was sputtered in a glove-box on the batches containing 2 ppm and 10 ppm of water. A batch containing 100 ppm of water was also prepared. However, the high water content in the ionic liquid leads to high outgassing and to high vacuum pressure in the sputter chamber. Generally, a gas pressure lower than 0.2 mbar is required to start the argon plasma. To obtain a batch containing 100 ppm of water, dry ionic liquid was used for sputtering and water was added after sputtering (0.5 μL of water and 3.5 mL of dry IL suspension). In Fig. 8 the absorption spectra of three batches of ionic liquid with different water contents are plotted. In Fig. 9 the UV-VIS absorption spectra after 24 hours of the different samples are plotted (top). Also the decrease in absorbance at 520 nm as a function of time is plotted which is a measure of the sedimentation speed (Fig. 9, bottom). The batch with 100 ppm of water shows more increase in absorbance at higher wavelengths (Fig. 9, top) and faster decrease in absorbance at 520 nm (Fig. 9, bottom) than the batch with 10 ppm of water, which in turn shows more coagulation and faster sedimentation than the batch with 2 ppm of water.

Attractive and repulsive forces

The DLVO theory was used to model the forces between two gold nanoparticles. An approximate expression for the electrostatic repulsion potential $V_{ele}(d)$ is:[30]

$$V_{ele}(d) = 2\pi r\varepsilon_0\varepsilon\psi_0^2 \ln[1 + \exp(-\kappa d)] \quad (1)$$

where ε_0 is the permittivity of free space, ψ_0 is the surface potential, κ is the reciprocal Debye length, r is the particle radius and d is the distance between the particle surfaces. The Debye reciprocal length κ is given by:[31]

$$\kappa = (N_A e^2 C_{eff}/\varepsilon_0\varepsilon k_B T)^{1/2} \quad (2)$$

κ was calculated by using the effective ionic charge concentration of the ILs (C_{eff} in mol m^{-3}), electronic charge (e), Boltzmann's constant (k_B) and Avogadro's number (N_A).

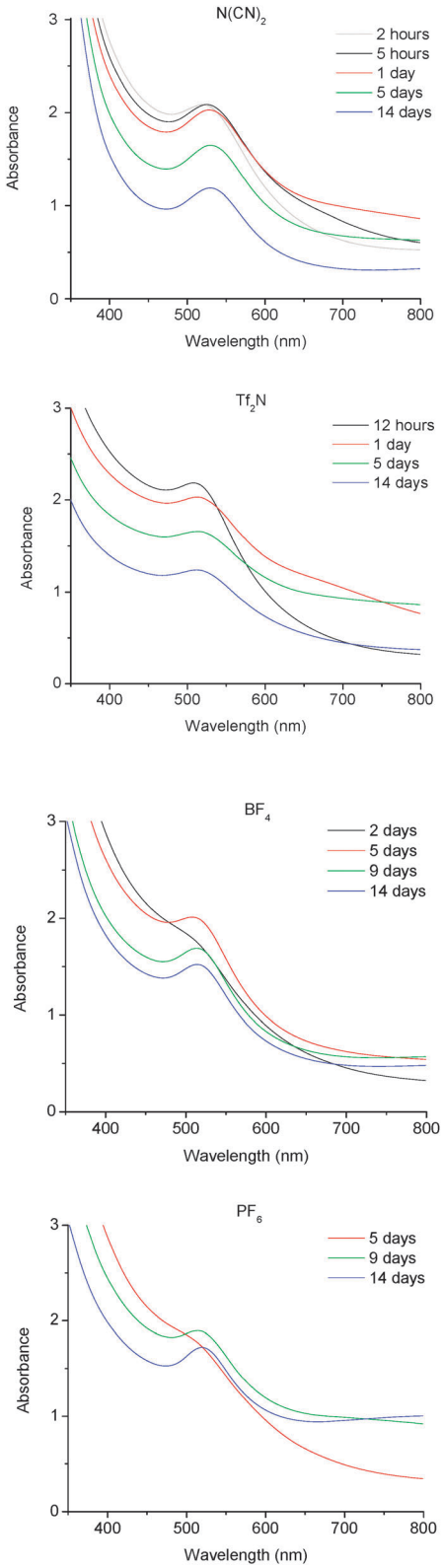

Fig. 5 UV-VIS absorption spectra of gold nanoparticles dispersed in ionic liquids $[C_1C_4Im][N(CN)_2]$, $[C_1C_4Im][Tf_2N]$, $[C_1C_4Im][BF_4]$ and $[C_1C_4Im][PF_6]$ as a function of time after sputter deposition. The spectra have been recorded at room temperature in a closed quartz cuvette.

A static permittivity (ε) of 11 is used to calculate $V_{ele}(d)$ and κ.[32] In ionic liquids, the zeta potential is a good approximation of the surface potential ψ_0, because of the high ionic strength. Zeta potentials of 5 to −55 mV are found in literature for NPs in imidazolium ionic liquids.[31] A value of −55 mV was selected for our calculations, which is likely to overestimate the electrostatic repulsion. The electrostatic potential between two gold NPs in an ionic liquid (1) is plotted as a function of interparticle distance in Fig. 10, expressed in units of kT. In the DLVO theory, this repulsive double layer attraction is offset by

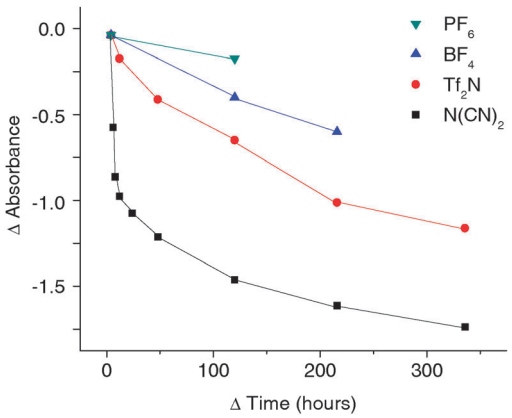

Fig. 6 Change in absorbance at 520 nm for different ionic liquids as a function of time. Time is set to zero when sedimentation starts. Lines are drawn between data points to guide the eye.

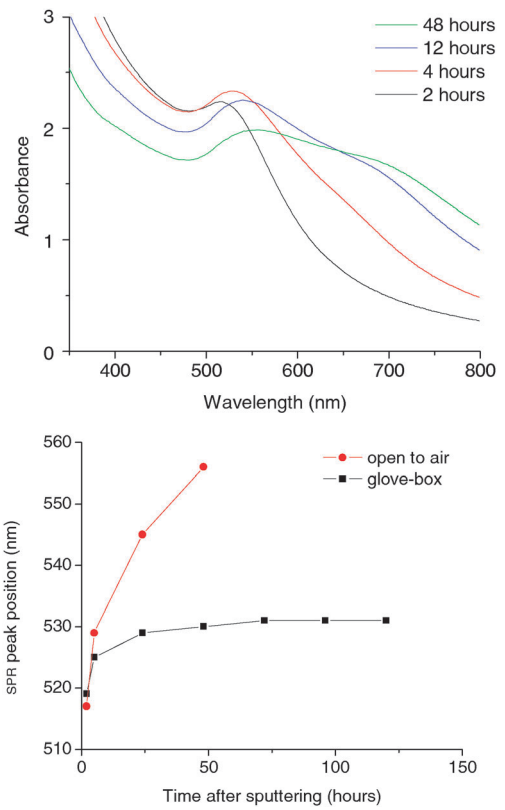

Fig. 7 UV-VIS absorption spectra of gold nanoparticles dispersed in the ionic liquid $[C_1C_4Im][N(CN)_2]$ as a function of time after sputter deposition (top). The position of the maximum of the SPR band as a function of time is given for both wet and dry samples (bottom). The spectra have been recorded at room temperature in a cuvette open to the air.

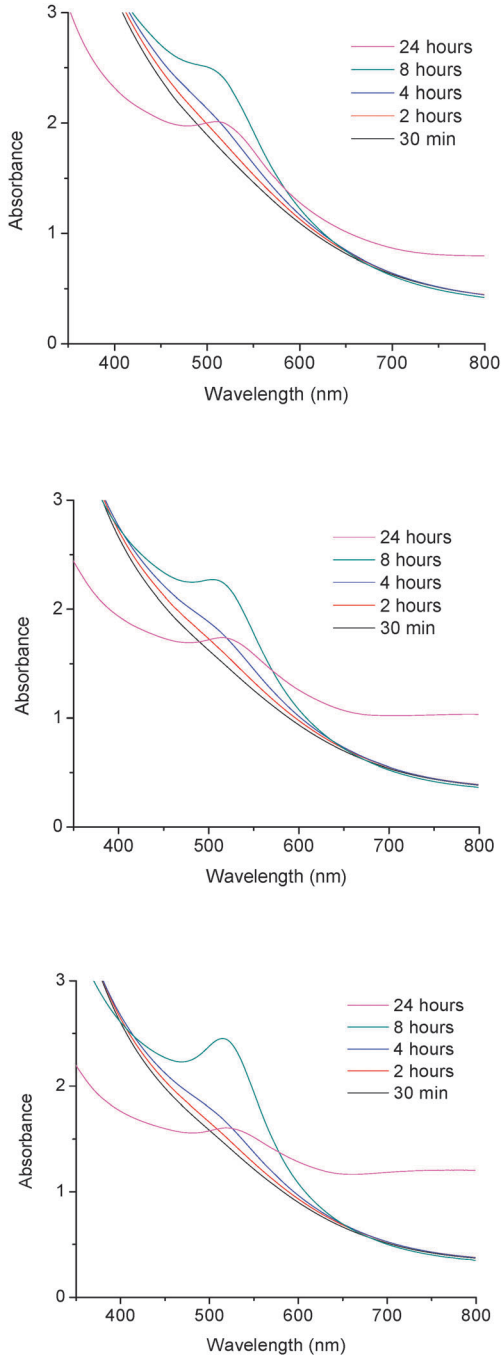

Fig. 8 UV-VIS absorption spectra of gold nanoparticles dispersed in the ionic liquid $[C_1C_4Im][Tf_2N]$ with different water contents as a function of time. Top: 2 ppm, middle: 10 ppm, bottom: 100 ppm.

the attractive van der Waals attraction $V_{vdW}(d)$. The $V_{vdW}(d)$ potential between two spherical particles of radius r and Hamaker constant A_p in a medium with Hamaker constant A_m and at a distance d of each other can be approximated by:[16]

$$V_{vdW}(d) = -(\sqrt{A_m} - \sqrt{A_p})^2 r/(12d) \quad (3)$$

The Hamaker constant A_m for $[C_1C_4Im][Tf_2N] = 5.57 \times 10^{-20}$ J and the Hamaker constant A_p for gold $= 1.26 \times 10^{-19}$ J.[31,33] A plot of this potential (3) as a function of interparticle distance is shown in Fig. 10.

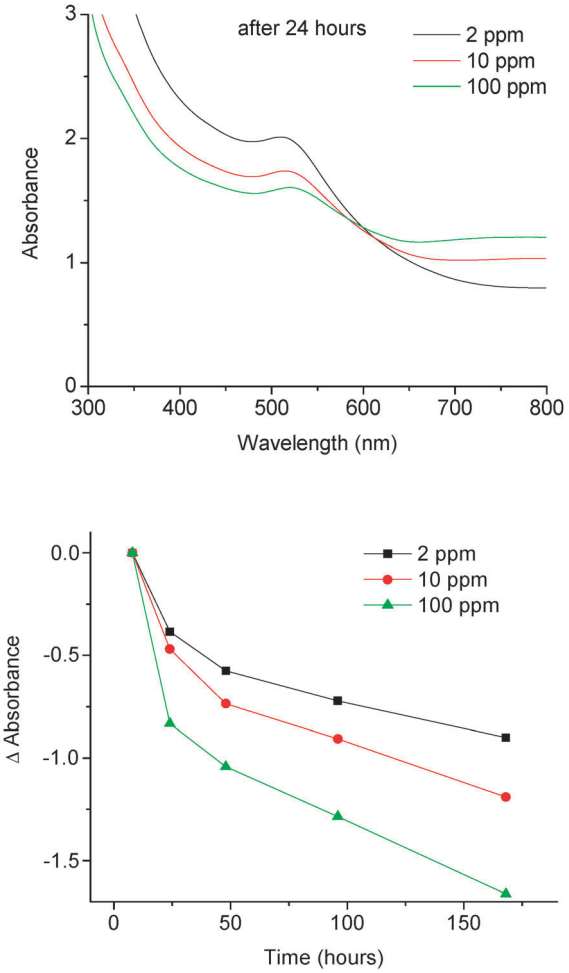

Fig. 9 UV-VIS absorption spectra of gold nanoparticles dispersed in samples of the ionic liquid $[C_1C_4Im][Tf_2N]$ with different water contents after 24 hours (top). Change in absorbance at 520 nm for different water contents as a function of time after sputter deposition (bottom).

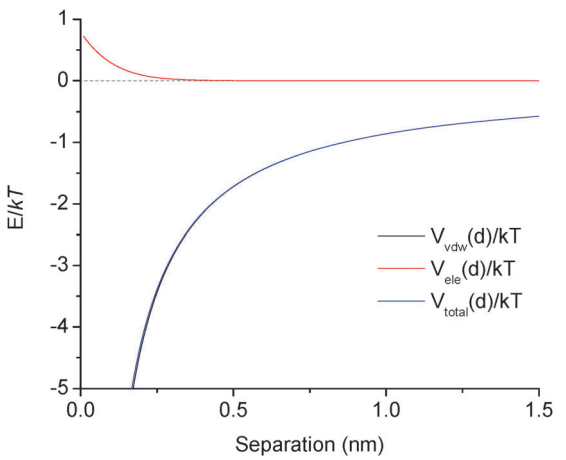

Fig. 10 $V_{total}(d) = V_{vdw}(d) + V_{ele}(d)$ as a function of distance between two spherical gold particles with a diameter of 6 nm. A dashed zero line is drawn for clarity.

One can see from Fig. 10 that the electrostatic repulsion only starts at 0.25 nm and is smaller than 1 kT over the whole distance range. The van der Waals attraction starts at distances of more

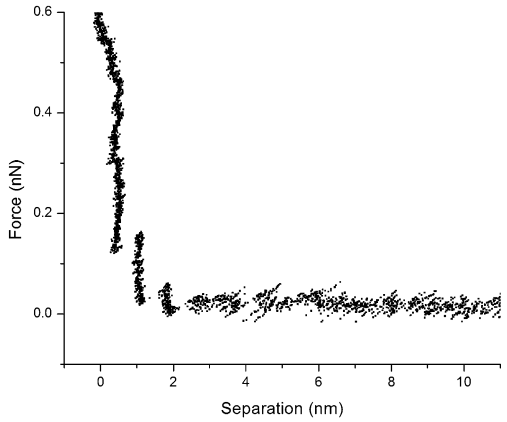

Fig. 11 AFM force–distance approach curve in $[C_1C_4Im][N(CN)_2]$ between a gold-coated AFM tip and a gold-coated mica surface.

than 10 nm and becomes larger than 1 kT at 1 nm interparticle distance. The total potential is negative over the whole distance range. To quantify the (un)stability predicted by DVLO theory, the $t_{1/2}$ time using the Smoluchowski equation was calculated

$$t_{1/2} = 3\eta/4k_bTN_0 \quad (4)$$

$t_{1/2}$ is the time when half of the particles have formed dimers. Eqn (4) assumes a sticking probability of 1, which means that when two Au NPs collide their chance of sticking together is 100%. The use of this simple form of the Smoluchowski equation is justified when we look at the interaction profile, $V_{total}(d)$, which is attractive at all distances (Fig. 10). Eqn (4) shows that $t_{1/2}$ is independent of the particle size and depends only on the viscosity of the IL and the NP concentration. Assuming that all the gold that is sputtered on the ionic liquid is converted to 5 nm gold NPs, a concentration of 1.2×10^{20} nanoparticles m^{-3} is obtained. The viscosity η of $[C_1C_4Im][Tf_2N]$ is 0.056 Pa s at 21 °C. The value of $t_{1/2}$ calculated using eqn (4) is 0.085 s.

To better understand the forces between two gold nanoparticles in an ionic liquid, force–distance measurements by AFM were done, between a gold coated AFM tip with a radius of *ca.* 40 nm and a gold coated mica surface (Fig. 11). The gold coating was formed by sputtering 60 nm of gold as measured by a quartz crystal microbalance (QCMB).

In the force distance curve in Fig. 11 a stepwise repulsive force is observed when the two gold coated surfaces approach each other within a few nanometres. This can be attributed to the layering of ILs next to a smooth surface. Layering is the arrangement of molecules or ions into discrete layers adjacent to a smooth solid surface due to entropic contributions. The observed stepwise force–distance curves are in agreement with literature data.[34,35]

Discussion

Coagulation and sedimentation

It was observed that besides the growth of the gold nanoparticles,[19] two other processes take place after sputtering of gold onto an ionic liquid, namely coagulation and sedimentation (Fig. 1). In Fig. 3 the large peak around 530 nm is attributed to the dipole plasmon resonance of the single gold NPs.[29] The increase in absorption from 5 min to 2 hours is attributed to the increase in the concentration of single gold NPs due to the coalescence of individual gold atoms or clusters that have been deposited in the ionic liquid by sputtering.[19] Between 2 and 24 hours, this peak height remains constant, which is due to the kinetic equilibrium between the formation of new gold NPs from individual gold atoms and the aggregation of NPs, which shifts the plasmon band to higher wavelengths. The smaller peaks at wavelengths between 600 and 800 nm, that develop during this time, are attributed to dipole plasmon excitations in coupled (*i.e.* aggregated) spheres.[29] Eventually, after 24 hours, the peak height of the main plasmon band at 530 nm decreases as the formation rate of new NPs cannot keep pace with the aggregation kinetics. It can be seen that the peaks in the longer wavelength region increase in height as a function of time. When a sol is colloidally unstable (*i.e.* the rate of aggregation is not negligible), the formation of aggregates is called coagulation. The increase in absorbance at higher wavelengths (600–800 nm) indicates that aggregates are being formed.[29] Also the broadening and the small shift of the plasmon resonance attributed to the single NP at 530 nm indicate the creation of larger nanoparticles and formation of aggregates. It is known that the SPR band is influenced by the nature of the metal, the size and shape of the nanoparticles and the surrounding medium.[36] Additionally, the SPR band is also sensitive to the interparticle distance. When nanoparticles approach each other close enough, the plasmons will interact with each other and cause a shift and broadening of the resulting SPR band or even give rise to a second SPR peak.[29] Because the nanoparticles are getting close to each other upon aggregation, an increase in the absorbance in the longer wavelength region is observed.[37] The aggregation process observed by UV-Vis absorption spectroscopy was confirmed by the corresponding TEM images. It can be seen in Fig. 2 that after two hours mainly single nanoparticles can be observed in the TEM images, while after 6 hours an amount of small aggregates had formed. After 24 hours larger aggregates with an average size of 200 nm were observed together with a large number of single NPs. Care must be taken when drawing conclusions from TEM images, because the aggregates observed in the TEM images might not represent the situation in bulk solution. Isolated NPs might cluster together and form aggregates during the TEM sample preparation. We believe that two-dimensional (2D) aggregates, with only one single layer of NPs, are promoted on the TEM grid, where the IL thickness becomes very thin perpendicular to the grid plane. 3D aggregates (spherical aggregates) are more likely to form in the bulk phase of the IL where the NPs are in an isotropic environment. When comparing the experimental spectra with the electrodynamic models in Fig. 4 we can see that SPR peaks shift to longer wavelengths when aggregates grow larger. To account for peak shifts up to 800 nm the aggregates must grow to a size about 20^3 NPs. This is an aggregate with a diameter of 150 nm. These results correspond with our observations of larger aggregates in the TEM images (Fig. 2).

Influence of the ionic liquid anion

In Fig. 5 it can be seen that coagulation starts 2 hours after sputtering for $[C_1C_4Im][N(CN)_2]$. For $[C_1C_4Im][Tf_2N]$,

Table 1 Viscosities of ionic liquids used in this study[a]

Ionic liquid	Viscosity/Pa s
$[C_1C_4Im][N(CN)_2]$	0.032
$[C_1C_4Im][Tf_2N]$	0.056
$[C_1C_4Im][BF_4]$	0.095
$[C_1C_4Im][PF_6]$	0.354

[a] The viscosities were measured at 21 °C and the water content of the ILs was lower than 30 ppm.

$[C_1C_4Im][BF_4]$ and $[C_1C_4Im][PF_6]$ coagulation starts after 12 hours, 2 days, and 5 days, respectively. When we compare these observations with the viscosity of the ionic liquids (Table 1) we see that the coagulation rate is inversely proportional to the viscosity of the ionic liquid.

The decrease in the overall absorbance value of the absorption spectra while maintaining the same shape indicates that sedimentation is occurring (Fig. 1). According to the law of Lambert–Beer the absorbance is directly proportional to the concentration of the absorbing species.[38] This means that the NPs are slowly being removed from the suspension. Sedimentation is the settling of suspended particles under the action of gravity. For $[C_1C_4Im][N(CN)_2]$, this process starts after 24 hours (Fig. 2). Also in this case the settling speed is slower as the viscosity of the ionic liquid is increased. This is visualised in Fig. 6 where the decrease in absorbance at 520 nm is plotted as a function of time. The sedimentation of the gold nanoparticles can be explained by Stokes' law, which predicts the settling velocity v of small spheres in a stagnant fluid:[39]

$$v = 2(\rho_p - \rho_f)gr^2/9\eta \quad (5)$$

where ρ is the density (the subscripts p and f indicate particle and fluid, respectively), g is the acceleration due to gravity (9.8 m s^{-2}), r is the radius of the particle and η is the dynamic viscosity of the fluid. In our example, $\rho_p = 19.3 \times 10^3$ kg m^{-3}, $\rho_f = 1.3 \times 10^3$ kg m^{-3}, $r = 3 \times 10^{-9}$ m, $\mu = 0.038$ kg m^{-1} s^{-1} for $[C_1C_4Im][N(CN)_2]$. This gives a settling velocity of $v = 0.92 \times 10^{-11}$ m s^{-1} or 1 cm in 34 years! If only single nanoparticles with radii up to 3 nm are taken into account, one can see that the settling velocity is so slow that the solution can be considered as a long-term stable suspension. However, according to the absorption spectra, precipitation already starts after one day in $[C_1C_4Im][N(CN)_2]$. For this to happen, the size of the particles or aggregates should be of the order of 200 nm. No nanoparticles larger than 7 nm were found in the TEM images, but large aggregates with an average size of 200 nm are observed by TEM. Consequently, the large aggregates are held responsible for the observed sedimentation.

Influence of water

As can be seen in Fig. 7, the red-shift of the SPR peak of the 'open' sample shifts rapidly to longer wavelengths, indicating that more intense aggregation is occurring. The formation of aggregates was confirmed by TEM analysis of the sample. In addition, the increase in absorption in the longer wavelength region is much more pronounced in the 'open' sample compared to the dry sample. The gold nanoparticles in the 'open' sample have completely sedimented after 7 days. The ionic liquid turned almost colourless and the gold had precipitated as a black sediment at the bottom of the cuvette. The water content after 7 days was 2500 ppm, as determined by Karl Fischer titration. These results clearly show that water plays an important role in the destabilization of gold nanoparticle sols in ionic liquids. From Fig. 9, it is evident that after 24 hours more drastic aggregation has occurred when more water was present in the sample. The batch with 100 ppm of water shows more coagulation (Fig. 9, top) and faster sedimentation (Fig. 9, bottom) than the batch with 10 ppm of water, which in its turn shows more coagulation and faster sedimentation than the batch with 2 ppm of water. This indicates that even a very small amount of water has a strong influence on the nanoparticle stability. The amount of water present is too small to attribute the differences in stability to changes in viscosity. 100 ppm of water equals a mole fraction of 2.3×10^{-3} in $[C_1C_4Im][Tf_2N]$ and this is expected to lead to a reduction of 0.64 mPa s in viscosity (or 1.1%).[40] If the influence of water is not a bulk phenomenon, the explanation has to be sought on the molecular scale, *i.e.* the interaction between water molecules and gold nanoparticles. A clean gold surface is known to be hydrophilic.[41] When the concentration of gold nanoparticles and the concentration of water molecules are compared, one finds that the concentration of gold equals 150 μg of Au per g IL (320 μmol of Au per mol IL) after 1 min sputtering and that the concentration of water (10 ppm) equals 10 μg H_2O per g IL (232 μmol of H_2O per mol IL). The concentration of gold NPs can be calculated by dividing the concentration of gold with the number of atoms per nanoparticles.[42] A gold nanoparticle with a diameter of 5 nm contains approximately 4000 gold atoms. Hence, at a water content of 10 ppm, every nanoparticle can be surrounded by 3000 water molecules which is enough to cover their surface for *ca.* 70%. This large water-to-gold NP ratio in combination with the hydrophilic behaviour of gold can cause a high concentration of water molecules near a NP and influence the stabilizing force of the ionic liquid surrounding the NP (*vida infra*). This hypothesis would explain the observed significant influence of very small amounts of water on the stability of gold nanoparticles.

Attractive and repulsive forces

It can be seen in Fig. 10 that the electrostatic repulsion only starts at 0.25 nm and is smaller than 1 kT, thus easily overcome by thermal motion of the NPs. In contrast, the attractive force already starts at distances of more than 10 nm and becomes larger than 1 kT from a distance of 1 nm. The total potential is negative over the whole distance range and indicates that no repulsive or stabilizing force is present. This indicates that the gold nanoparticle suspension is very unstable. To quantify this unstability the $t_{1/2}$ time using the Smoluchowski equation was calculated. $t_{1/2}$ is the time after which half of the particles have formed dimers. According to this calculation ($t_{1/2} = 0.085$ s), flocculation should occur almost instantly. This contradicts with the experimental results. The suspension is found to be stable over time periods of a few hours or days depending on the viscosity of the ionic liquid (Fig. 1 and 2). This indicates that the suspension is more stable than the theoretical $t_{1/2}$ suggests. This means there is another repulsive

force present besides the electrostatic double layer force, preventing the fast destabilization of the sol. From the AFM force–distance measurements with a gold coated cantilever and a gold-coated mica surface, an oscillatory repulsive force is observed between the two gold surfaces (Fig. 11) which is due to layering of the ionic liquid and which strongly reduces the sticking probability when particles collide. The formation of a layer of ionic liquid surrounding a metal nanoparticle in an ionic liquid was proposed by Dupont and co-workers.[43] These authors showed by surface enhanced Raman scattering (SERS) that the imidazolium ions are present with the aromatic ring in an orientation parallel to the nanoparticle surface. The anions do not interact directly with the metal nanoparticle and are located in the second coordination sphere. It was observed in this study that imidazolium ILs exhibit a similar stability behaviour. On the other hand, the anions are responsible for differences in viscosity and therefore influence the kinetics. This would lead one to conclude that the anions, for the ILs used in this study, only play a secondary role in the stabilisation of the gold nanoparticles by changing the viscosity. However, comparison of Fig. 5 with Table 1 shows that the stability of the coagulation process does not scale linearly with viscosity and hence we would like to conclude that the anions not merely play a role in changing the viscosity but also influence the structural forces that determine the coagulation rate of nanoparticles. The presence of a stabilizing layer of ionic liquid surrounding the gold nanoparticles explains the observations made in this study that the nanoparticle suspensions are relatively stable in contrast to the predicted instability by the DVLO theory. It also explains the observation that NP aggregates do not sinter to form bulk gold. The observed aggregates are a collection of NPs in close contact with each other but which remain separated by a distance of approximately 0.5 nm (Fig. 2). This suggests that a layer of ionic liquid remains present around the NPs. This occurs because the attractive dispersion forces bring the particles together, but these forces are not strong enough to destabilize the last few layers of structured ionic liquid. This also explains the strong influence water has on the stability of these nanoparticles. The presence of water near the gold surface probably disrupts the ionic liquid layers which decreases the structural solvation forces.

Due to the clean synthesis method used, the sole species present in solution besides gold are the ionic liquid ions. This offers a major advantage compared to other synthesis techniques, which use metal precursors or reducing agents that introduce impurities in the IL/NP system and might influence the stability of the NPs.

Conclusions

It was found that two processes after the sputter deposition of gold on an ionic liquid occur. First, growth of nanoparticles from the sputtered Au atoms or clusters occurs until nanoparticles with a diameter of about 5–6 nm are formed.[19] As these nanoparticles are formed, coagulation of the NPs takes place and, as a consequence, these aggregates start to settle. It was shown that the viscosity of the ionic liquid has an influence on the kinetics of these processes. The more viscous the IL, the slower are the kinetics of the coagulation and sedimentation. Generalized multiparticle Mie calculations showed that the increase in absorbance at wavelengths from 600 to 800 nm can be attributed to the formation of large aggregates containing more than 10^3 NPs. Water was found to have a major impact on the stability of the gold nanoparticle sol. Even very small amounts of water (ppm range) have an influence on the stability of gold NPs/IL suspensions. It was shown that electrostatic and van der Waals forces alone cannot account for the coagulation and sedimentation behaviour observed in this study. As no other species are present, the ionic liquid must play a role in the stabilization of the gold nanoparticles. The limited stabilisation provided by ionic liquids is probably not due to electrostatic forces, as frequently assumed, but rather due to solvation forces caused by the layering of the ionic liquid near the surface of the nanoparticles.

Acknowledgements

The authors acknowledge financial support by the KU Leuven (project IDO/05/005), the FWO-Flanders (research community "Ionic Liquids"), the IWT-Flanders (SBO-project "MAPIL"), the Belgian Federal Science Policy Office through the IUAP project INANOMAT (contract P6/17), and the Belgian Hercules Stichting (HER/08/25). Support by IoLiTec (Heilbronn, Germany) is also acknowledged.

References

1 P. Migowski and J. Dupont, *Chem.–Eur. J.*, 2007, **13**, 32–39.
2 V. I. Parvulescu and C. Hardacre, *Chem. Rev.*, 2007, **107**, 2615–2665.
3 L. S. Ott and R. G. Finke, *Coord. Chem. Rev.*, 2007, **251**, 1075–1100.
4 K. Ueno, H. Tokuda and M. Watanabe, *Phys. Chem. Chem. Phys.*, 2010, **12**, 1649–1658.
5 S. Kuwabata, T. Tsuda and T. Torimoto, *J. Phys. Chem. Lett.*, 2010, **1**, 3177–3188.
6 J. Dupont and P. A. Z. Suarez, *Phys. Chem. Chem. Phys.*, 2006, **8**, 2441–2452.
7 H. S. Schrekker, M. A. Gelesky, M. P. Stracke, C. M. L. Schrekker, G. Machado, S. R. Teixeira, J. C. Rubim and J. Dupont, *J. Colloid Interface Sci.*, 2007, **316**, 189–195.
8 Y. Wang and H. Yang, *Chem. Commun.*, 2006, 2545–2547.
9 H. Itoh, K. Naka and Y. Chujo, *J. Am. Chem. Soc.*, 2004, **126**, 3026–3027.
10 K.-S. Kim, S. Choi, J.-H. Cha, S.-H. Yeon and H. Lee, *J. Mater. Chem.*, 2006, **16**, 1315–1317.
11 J. Zhu, Y. Shen, A. Xie, L. Qiu, Q. Zhang and S. Zhang, *J. Phys. Chem. C*, 2007, **111**, 7629–7633.
12 K.-I. Okazaki, T. Kiyama, K. Hirahara, N. Tanaka, S. Kuwabata and T. Torimoto, *Chem. Commun.*, 2008, 691–693.
13 P. R. Dash and W. J. Scott, *Chem. Commun.*, 2009, 812–814.
14 B. Derjaguin and L. Landau, *Acta Physicochim. USSR*, 1941, **14**, 633–662.
15 E. J. Verwey and J. Th. G. Overbeek, *Theory of the stability of lyophobic colloids*, Elsevier, Amsterdam, 1948.
16 K. Ueno and M. Watanabe, *Langmuir*, 2011, **27**, 9105–9115.
17 S. Kuwabata, T. Tsuda and T. Torimoto, *J. Phys. Chem. Lett.*, 2010, **1**, 3177–3188.
18 T. Torimoto, K. Okazaki, T. Kiyama, K. Hirahara, N. Tanaka and S. Kuwabata, *Appl. Phys. Lett.*, 2006, **89**, 243117.
19 E. Vanecht, K. Binnemans, J. W. Seo, L. Stappers and J. Fransaer, *Phys. Chem. Chem. Phys.*, 2011, **13**, 13565–13571.
20 H. Wender, P. Migowski, A. F. Feil, L. F. Oliviera, M. H. G. Prechtl, R. Leal, G. Machado, S. R. Teixeira and J. Dupont, *Phys. Chem. Chem. Phys.*, 2011, **13**, 13552–13557.
21 K. Richter, A. Birkner and A. Mudring, *Angew. Chem., Int. Ed.*, 2010, **49**, 2431–2435.

22 K. Richter, A. Birkner and A. Mudring, *Phys. Chem. Chem. Phys.*, 2011, **13**, 7136–7141.
23 Y. L. Xu and R. T. Wang, *Phys. Rev. E*, 1998, **58**, 3931–3948.
24 Y. L. Xu, *Appl. Opt.*, 1997, **36**, 9496–9508.
25 P. B. Johnson and R. W. Christy, *Phys. Rev. B*, 1972, **6**, 4370–4379.
26 M.-C. Daniel and D. Astruc, *Chem. Rev.*, 2004, **104**, 293–346.
27 S. J. Guo and E. K. Wang, *Anal. Chim. Acta*, 2007, **598**, 181–192.
28 S. Link and M. A. El-Sayed, *J. Phys. Chem. B*, 1999, **103**, 8410–8426.
29 Z. Zhong, S. Patskovsky, P. Bouvrette, J. H. T. Luong and A. Gedanken, *J. Phys. Chem. B*, 2004, **108**, 4046–4052.
30 S. L. Carnie and D. Y. C. Chan, *J. Colloid Interface Sci.*, 1993, **161**, 260–264.
31 K. Ueno, A. Inaba, M. Kondoh and M. Watanabe, *Langmuir*, 2008, **24**, 5253–5259.
32 I. Krossing, J. M. Slattery, C. Daguenet, P. J. Dyson, A. Oleinikova and H. Weingärtner, *J. Am. Chem. Soc.*, 2006, **128**, 13427–13434.
33 C. Argento and R. H. French, *J. Appl. Phys.*, 1996, **80**, 6081–6090.
34 R. Atkin and G. Warr, *J. Phys. Chem. C*, 2007, **111**, 5162–5168.
35 D. Wakeham, R. Hayes, G. Warr and R. Atkin, *J. Phys. Chem. B*, 2009, **113**, 5961–5966.
36 S. K. Gosh and T. Pal, *Chem. Rev.*, 2007, **107**, 4797–4862.
37 C. D. Keating, M. D. Music, M. H. Keefe and M. J. Natan, *J. Chem. Educ.*, 1999, **76**, 949–955.
38 J. D. J. Ingle and S. R. Crouch, *Spectrochemical Analysis*, Prentice Hall, New Jersey, 1988.
39 G. G. Stokes, *Trans. Cambridge Philos. Soc.*, 1843, **8**, 287–341.
40 K. R. Seddon, A. Stark and M. J. Torres, *Pure Appl. Chem.*, 2000, **72**, 2275–2287.
41 T. Smith, *J. Colloid Interface Sci.*, 1980, **75**, 51–55.
42 X. Liu, M. Atwater, J. Wang and Q. Huo, *Colloids Surf., B*, 2007, **58**, 3–7.
43 J. C. Rubim, F. A. Trindade, M. A. Gelesky, R. F. Aroca and J. Dupont, *J. Phys. Chem. C*, 2008, **112**, 19670–19675.